Structure and nuclear quadrupole coupling interaction in hydroxylamines: The rotational spectrum of *N,N*-diethyl(²H)hydroxylamine

Filippo Baroncelli [a,1], Gabriele Panizzi [a,1], Luca Evangelisti [b,c,d,1], Sonia Melandri [a,c,d,1], Assimo Maris [a,d,*,1]

[a] *Department of Chemistry "G. Ciamician", University of Bologna, Bologna 40126, Italy*
[b] *Department of Chemistry "G. Ciamician" - Campus of Ravenna, University of Bologna, Ravenna 40126, Italy*
[c] *Interdepartmental Centre for Industrial Agrifood Research (CIRI Agrifood), University of Bologna, Forlì 47121, Italy*
[d] *Interdepartmental Centre for Industrial Aerospace Research (CIRI Aerospace), University of Bologna, Cesena 47521, Italy*

ABSTRACT

The ground-state rotational spectrum of *N,N*-diethyl(²H)hydroxylamine (C_2H_5-NOD-C_2H_5) was measured by Fourier transform microwave spectroscopy. Six rotational transition lines were assigned to the most stable conformer with the alkyl chain in the *trans* arrangement and the hydroxyl *trans* to the bisector of the CNC angle, that is, with the NOD frame in the *bc*-symmetry plane. Rotational constants are $A = 7210.938(2)$, $B = 2018.628(1)$, and $C = 1739.696(1)$ MHz. These data together with those previously determined for the parent species and ^{13}C and ^{15}N isotopologues, were used to determine a partial r_0 structure. The hyperfine structure due to the nuclear quadrupole coupling (NQC) interaction of both ^{14}N and D nuclei was disentangled allowing to obtain the diagonal NQC-constants. On the basis of the determined geometry, the NQC-tensor values in the electric field-gradient principal axis system were determined ($\chi_{xx}^N = 0.71$, $\chi_{yy}^N = 5.90$, $\chi_{zz}^N = -6.61$ MHz; $\chi_{xx}^D = -0.11$, $\chi_{yy}^D = -0.15$, $\chi_{zz}^D = 0.26$ MHz). Comparison with other amines shows that using ammonia as reference, χ_{zz}^N can be estimated with an additive model: $+0.4$ and $+1.7$ MHz from hydrogen to alkyl and hydroxyl substitution, respectively. From the analysis of the available data on the 1:1 water complex of *N,N*-diethylhydroxylamine, a 8% electric field gradient decrease at the nitrogen nucleus due to the formation of the hydrogen bond involving the nitrogen lone pair was found.

1. Introduction

Nowadays, hydroxylamine derivatives are commonly found in many different industrial applications. They are used as initiators for the Nitroxide-Mediated Polymerization (NMP), to produce a polymer with a controlled architecture [1]. They are found as intermediates of the Denisov cycle, a catalytic cycle occurring in plastic added with Hindered Amine Light Stabilizers (HALS) additives in order to prevent photo-degradation [2]. Their application is based on their peculiar properties given by the presence of the NO bond, which makes the formation of the relatively stable aminoxyl radical possible. However, the overall molecular structure affects the stability of the radical itself [3]. For instance, TEMPO ((2,2,6,6-tetramethylpiperidin-1-yl)oxy) is a particularly stable radical where the additional stability is attributed to the steric protection provided by the four methyl groups

adjacent to the aminoxyl group and the absence of hydrogen atoms in *α* position [4]. Due to their propensity to cleave homolytically, hydroxylamine derivatives have been also considered as possible theranostic agents [5].

With the purpose of modelling and characterizing the structural and electronic properties of the hydroxylamine group, we have recently investigated *N,N*-diethylhydroxylamine (DEHA) in the gas phase using a multi-spectral approach based on rotational, near-infrared, valence band and core photoionization and near edge X-ray absorption fine structure spectroscopies [6]. We have proved that the three most stable conformers are characterized by the hydroxyl hydrogen atom being in the *trans* orientation with respect to the bisector of the CNC angle while the side alkyl chains can be both *trans* or one *trans* and the other *gauche* or *gauche'*. The global minimum, shown in Fig. 1, is the *all-trans* form, which presents a C_s-symmetry where the plane
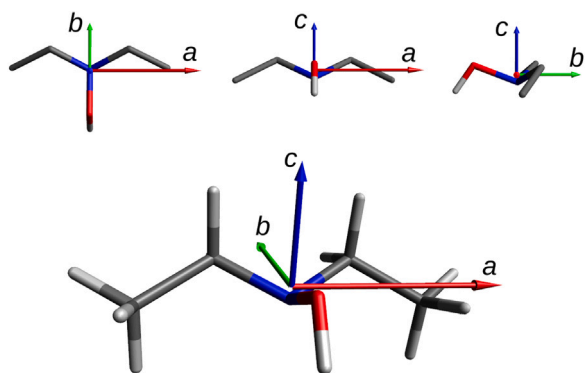
Fig. 1. Structure of the most stable conformer of DEHA and principal inertial axis system. The *bc*-plane is a symmetry plane.

symmetry corresponds to the *bc*-plane. For this conformer, the ^{13}C and ^{15}N isotopologues were observed in natural abundance, allowing for a partial structure determination. Moreover, we observed its 1:1 water complex [7]. The water molecule lies in the *bc* symmetry plane forming two hydrogen bonds with the NOH frame, leading to an overall C_s symmetry species. Rather surprisingly, the hydrogen bond where the electronegative acceptor atom is nitrogen is shorter and stronger than the hydrogen bond where the electronegative acceptor atom is oxygen.

Important information on the electron distribution is encoded in the nuclear quadrupole coupling (NQC) tensor ($\chi^{3\times3}$) which is related to the electric field gradient (EFG) tensor ($q^{3\times3}$) at the involved nucleus by:

$$\begin{bmatrix} \chi_{xx} & \chi_{xy} & \chi_{xz} \\ \chi_{yx} & \chi_{yy} & \chi_{yz} \\ \chi_{zx} & \chi_{zx} & \chi_{zz} \end{bmatrix} = e \cdot \begin{bmatrix} q_{xx} & q_{xy} & q_{xz} \\ q_{yx} & q_{yy} & q_{yz} \\ q_{zx} & q_{zx} & q_{zz} \end{bmatrix} \cdot Q \tag{1}$$

where e is the elementary charge, the q elements are the second derivative of the electrostatic potential (i.e. $q_{xy} = \partial^2 V / \partial x \partial y$) and Q is the conventional nuclear electric quadrupole moment, all of which are known constants. For instance, the changes of the NQC-tensors at the chlorine and bromine atoms which take place upon perfluorination of aryl halides is a direct measure of the extent of the σ hole at the tip of the halogen atom [8].

Here we extend the study to the hydroxyl deuterated form (*N,N*-diethyl(^{2}H)hydroxylamine, DEDA from now on) in order to obtain more insights on the molecular structure. Moreover, by means of the extremely high resolution of Fourier transform microwave spectroscopy, we want to resolve the hyperfine structure due to the interaction between the nuclear quadrupole moments of the nitrogen (^{14}N) and deuterium atoms, with the end-over-end rotation of the molecule, in order to determine their NQC-tensors.

2. Experimental methods

DEHA ($C_4H_{11}NO$, CAS Registry Number: 3710-84-7) was purchased from Merck with a declared minimum purity of 98%. It is a colourless to light yellow liquid, miscible in water and with an ammoniacal odour. Declared properties are: vapour pressure 0.53 kPa at 273.15 K, melting point 247–248 K, and boiling point 398–403 K. Deuterium oxide (D_2O, CAS Registry Number: 7789-20-0) was purchased from Cambridge Isotope Laboratories, Inc with declared isotopic purity of 99.9%. Helium was purchased from SIAD (Società Italiana Acetilene e Derivati). All the compounds were used without further purification. The gas phase sample was studied in supersonic expansion conditions, which allow for efficient cooling of the rotational degrees of freedom. In order to substitute the hydroxyl hydrogen with deuterium, the sample was initially prepared as a mixture of DEHA and D_2O (3:1 in volume). Due to the adsorption of D_2O into the pneumatic injection system, the

addition of D_2O was no more necessary and deuterated samples were obtained by the exchange reaction between DEHA and D_2O adsorbed on the walls of the pre-expansion apparatus. The spectrum was measured in the 6.5–18.5 GHz frequency region by means of a pulsed jet Fourier transform microwave (PJ-FTMW) spectrometer (COBRA-type [9,10]), whose details have been described previously [11]. Helium at a stagnation pressure of 0.4 MPa was passed over the sample kept at room temperature and expanded through a solenoid valve (General Valve, Series 9, nozzle diameter 0.5 mm) into the Fabry–Pérot cavity. The spectral line positions were determined after Fourier transformation of the time-domain signal with 8 k data points, recorded with 100 ns sample intervals. Each rotational transition appears as a doublet due to the Doppler Effect and the line position is calculated as the arithmetic mean of the frequencies of the Doppler components. The estimated accuracy of the frequency measurements is better than 3 kHz and lines separated by more than 7 kHz are resolvable. The rotational temperature of the molecules in the pulsed jet was estimated to be about 1 K.

3. Computational details

Quantum mechanical calculations were carried out using the GAUSSIAN16® software package (G16, Rev. A.03[2]) by means of both density functional theory (DFT) and *ab initio* methods. As regards DFT, the valence triple-zeta quality Karlsruhe polarized type basis set (def2-TZVP [12]) was used in combination with the Becke-three-parameters Lee-Yang-Parr hybrid density functional (B3LYP [13,14]) corrected by the D3 version of Grimme's empirical dispersion with Becke–Johnson damping (B3LYP-D3(BJ) [15,16]). As for the *ab initio* approach, the valence triple-zeta quality Dunning correlation consistent polarized type basis set augmented with diffuse functions (aug-cc-pVTZ [17]) was used in combination with the Møller–Plesset second-order perturbation theory (MP2 [18]).

The angular distribution of the EFG tensors was calculated using the code provided by Autschbach et al. [19] and visualized by means of the numerical analysis software Wolfram Mathematica [20]. Briefly, a scalar function $f(x, y, z)$ centred on a specific atom is calculated as:

$$f(x, y, z) = \begin{pmatrix} x & y & z \end{pmatrix} \times q^{3\times3} \times \begin{pmatrix} x \\ y \\ z \end{pmatrix} \tag{2}$$

where x, y and z are the cartesian coordinates and $q^{3\times3}$ is the EFG-tensor. The $f(x, y, z)$ function is then expressed in spherical coordinates (r, θ and ϕ), obtaining:

$$f(r, \theta, \phi) = r^2 \cdot g(\theta, \phi) \tag{3}$$

where the $g(\theta, \phi)$ function represents the angular dependence of the function. Finally, the EFG tensor is shown as a polar plot of $g(\theta, \phi)$, and different colours are used depending on the positive or negative value of the function $g(\theta, \phi)$.

4. Rotational spectrum

Three μ_b^R-type and three μ_c^R-type rotational transition lines with lower $J = 0 - 2$ and $K_a = 1 \leftarrow 0$ were observed for the *all-trans* conformer. All the lines show a hyperfine structure due to the nuclear quadrupole coupling interaction of ^{14}N and D. As an example, the $2_{1,1} - 1_{0,1}$ transition line is shown in Fig. 2.

The assignment and the fit were performed using the CALPGM software, which includes the SPFIT and SPCAT programs for the fitting and the prediction of the spectral lines, respectively [21]. Measured transition lines were fitted to Watson's *S*-reduced semirigid asymmetric rotor
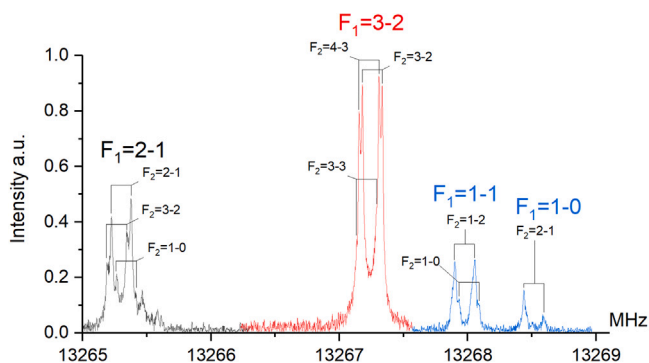

Fig. 2. A typical high-resolution measurement of the $2_{1,1} - 1_{0,1}$ rotational transition of DEDA. The Doppler doubling is marked by brackets and the NQC components are given. Different colours indicate different excitation frequencies.

Hamiltonian [22] in the I^r representation and including the nuclear quadrupole coupling terms:

$$\hat{H} = \hat{H}_R + \hat{H}_{CD} + \hat{H}_Q^N + \hat{H}_Q^D \tag{4}$$

where $\hat{H}_R$ represents the rigid rotor Hamiltonian related to the A, B and C rotational constants, $\hat{H}_{CD}$ takes into account the centrifugal distortion effect, and $\hat{H}_Q$ are the operators associated with the quadrupole interaction of the ^{14}N nuclear spin ($I = 1$) and D nuclear spin ($I = 1$). Since the nuclear quadrupole moment of deuterium ($Q = 0.28578(3)$ e·fm^2 [23]) is about one order of magnitude lower than that of nitrogen ($Q = 2.044(3)$ e·fm^2 [24]), the splitting of the rotational levels caused by deuterium is smaller than that caused by ^{14}N. For this reason, the following sequential coupling of the angular momenta was adopted:

$$\vec{F}_1 = \vec{J} + \vec{I}_N \qquad \vec{F}_2 = \vec{F}_1 + \vec{I}_D \tag{5}$$

The assigned lines are reported in Table 1 and the fitted constants in Table 2.

5. Structure

Due to the molecular C_s-symmetry, the NOH frame lies in the bc-plane. Hence, at the equilibrium geometry, the a-coordinate for the N, O and H atoms is expected to be null and the planar moment of inertia along the a-axis ($M_{aa} = \sum_i m_i \cdot a_i^2$) is expected to be the same for the parent species and the ^{15}N and hydroxyl deuterated species. However, in the vibrational ground state, molecular motions affect the atomic positions and small displacements from the expected values can be found. In Table 3 the planar moments of inertia of DEDA are compared to those of DEHA and its ^{13}C and ^{15}N monosubstituted isotopologues [6]. Actually, the M_{aa} value of DEDA is only 0.005 uÅ^2 smaller than that of DEHA and 0.009 uÅ^2 bigger than that of DEHA-^{15}N, further proving that the hydroxyl lies in the symmetry plane.

The rotational constants of DEDA and those of DEHA [6] were used to calculate the absolute substitution coordinates of the hydroxyl hydrogen atom using Kraitchman's equations [26] and Costain's model [25] to derive the errors. They are compared to the theoretical equilibrium coordinates in Table 4. However, Kraitchman's method assumes a rigid isotopically invariant molecular geometry. Probably due to the contribution of the zero-point vibrational motions, an imaginary value is obtained for $|a_s|$ instead of the expected null value. This effect is similar to that observed in planar molecules in which out-of-the-plane movement of the atoms results in substitution coordinates that represent the root-mean-square average vibrational displacements [27]. $|b_s|$ is smaller than the $|b_e|$ obtained at the B3LYP-D3(BJ)/Def2-TZVP level of calculation by 0.005 Å, and bigger than the $|b_e|$ obtained at the MP2/aug-cc-pVTZ level of calculation by 0.002 Å. $|c_s|$ is smaller than both theoretical values, by 0.016 and 0.013 Å for B3LYP-D3(BJ)/Def2-TZVP and MP2/aug-cc-pVTZ, respectively. As already found for the

coordinates of the nitrogen and carbon atoms in [6], a good agreement between the experimental and theoretical data is found, the match being better with MP2/aug-cc-pVTZ than B3LYP-D3(BJ)/Def2-TZVP. In the same article, we also show that despite the DFT approach providing rotational constants in better agreement with the values of the observed conformers of DEHA, the MP2 r_e-structure is more reliable.

Based on the latter considerations, the *ab initio* geometry has been chosen as the starting point for a structural fitting where a set of selected internal coordinates has been adjusted in order to reproduce the fifteen rotational constants of the five observed species. Since the available information allows only for the determination of a partial structure, several trials were done to determine the most suitable combination of parameters to be fitted and the choice was guided by the following criteria: avoiding overfitting, reproducing the rotational constants as well as possible, and obtaining the smallest uncertainties of the fitted parameters. Moreover, zero-point vibrational effects in bonds involving hydrogen or deuterium atoms are expected to give different average bond lengths. In agreement with Laurie [28], in order to take into account the vibrational contribution, here a 0.002 Å shortening of the OD bond length with respect to the OH one has been considered. The STRFIT [29] software has been used and the results obtained by changing the hydroxyl and the skeletal bond distances, are summarized in Table 5. It is worth noting that the hydroxyl and CN bond distances remain almost unchanged with respect to the theoretical values, whereas the NO and CC bond distances elongate by more than 0.01 Å.

6. ^{14}N-NQC constants

The experimental and *ab initio* ^{14}N NQC-constants of DEHA and DEDA are compared in Table 6. Due to the C_s symmetry of the molecule, the inertial principal axis system (I-PAS) and the electric field gradient principal axis system (EFG-PAS) must share a direction, which is the a-axis. As a consequence, the NQC-constant along the a-principal inertia axis of the parent species ($\chi_{aa} = 0.711(2)$ MHz) is expected to be equal to that of the deuterated one ($\chi_{aa} = 0.716(3)$ MHz). Actually, they are equal within the standard errors quoted. Moreover, DEHA and DEDA have only one off-diagonal NQC-constant different from zero (χ_{bc}). This term is related to the diagonalization angle θ, which describes the rotation of the b and c axes around the a-axis of the I-PAS to give the y and z axes of the EFG-PAS, by:

$$\tan(2\theta) = \frac{2 \cdot \chi_{bc}}{\chi_{bb} - \chi_{cc}} \tag{6}$$

Since we could not determine the experimental off-diagonal term from the fit, it is impossible to obtain the NQC-tensor in the EFG-PAS by direct diagonalization. Nevertheless, we can adopt a different approach, because we have information on both DEHA and DEDA. Indeed, upon diagonalization of the complete NQC-tensors in the I-PAS of DEHA and DEDA, the same NQC-tensor in the EFG-PAS must be obtained:

$$\chi_{EFG-PAS} = \begin{cases} R'^{DEHA} \times \chi_{I-PAS}^{DEHA} \times R^{DEHA} \\ R'^{DEDA} \times \chi_{I-PAS}^{DEDA} \times R^{DEDA} \end{cases} \tag{7}$$

where R are the rotation matrices. The difference between the rotation angles θ_{DEHA} and θ_{DEDA} is the tilt angle describing the rotation of the bc-axes that takes place upon deuteration. From the structure determined in the previous section, we know that this tilt angle is 1.3°. Using this constrain, the diagonalization angles that provide the same diagonal tensor are $\theta_{DEHA} = -10.6°$ and $\theta_{DEDA} = -11.9°$, respectively. The corresponding NQC-constants in the EFG-PAS are given in Table 6 with the asymmetry parameter η:

$$\eta = \frac{\chi_{xx} - \chi_{yy}}{\chi_{zz}} \tag{8}$$

Their values and associated errors were calculated using the QDIAG program supplied by Zbigniew Kisiel, available on the PROSPE website [30]. The same approach has been applied to determine the NQC-tensor in

Table 1

Experimental rotational transition frequencies of *N,N*-diethyl(^{2}H)hydroxylamine.

J''	K_a''	K_c''	F_1''	F_2''	–	J'	K_a'	K_c	F_1'	F_2'	$\nu_{obs.}$/MHz	$\nu_{obs.} - \nu_{calc.}$/MHz
1	1	1	0	1		0	0	0	1	2	8 947.946	−0.006
			2	3					1	2	8 950.362	−0.001
			1	2					1	2	8 951.971	−0.004
2	1	2	1	2		1	0	1	1	2	12 428.326	−0.000
			1	2					0	1	12 428.867	0.002
			3	4					2	3	12 429.623	0.001
			2	2					1	1	12 431.318	−0.001
			2	3					1	2	12 431.368	0.001
			2	3					2	3	12 431.567	−0.005
			2	2					2	2	12 431.592	0.001
3	1	3	2	3		2	0	2	1	2	15 773.153	0.001
			4	5					3	4	15 773.708	0.001
			3	4					2	3	15 775.501	0.001
1	1	0	1	2		0	0	0	1	2	9 228.052	0.004
			2	3					1	2	9 229.865	0.001
			2	2					1	1	9 229.891	0.002
			0	1					1	2	9 232.611	0.005
2	1	1	2	2		1	0	1	1	1	13 265.261	−0.001
			2	3					1	2	13 265.304	0.004
			2	1					1	0	13 265.341	0.001
			3	3					2	3	13 267.219	0.001
			3	4					2	3	13 267.231	0.001
			3	3					2	2	13 267.257	0.002
			1	1					1	2	13 267.979	0.004
			1	1					1	0	13 268.005	−0.007
			1	2					0	1	13 268.517	−0.003
3	1	2	4	3		2	0	2	3	2	17 447.967	−0.004
			4	5					3	4	17 447.980	0.002
			4	4					3	3	17 447.995	−0.003
			2	3					1	2	17 448.763	0.003

Table 2

Experimental and theoretical rotational spectroscopy parameters (in MHz, *S*-reduction, I^r representation) of *N,N*-diethyl(^{2}H)hydroxylamine.

	Exp.	DFT[a]	MP2[b]
A	7210.938(2)[c]	7198.445	7281.841
B	2018.628(1)	2017.939	2037.236
C	1739.696(1)	1738.805	1755.623
D_J	0.19(5)·10^{-3}	0.16·10^{-3}	0.16·10^{-3}
$1.5 \cdot \chi_{aa}^N$	1.075(5)	1.269	0.909
$(\chi_{bb}^N - \chi_{cc}^N)/4$	2.861(1)	3.121	2.791
$1.5 \cdot \chi_{aa}^D$	−0.232(7)	−0.276	−0.275
$(\chi_{bb}^D - \chi_{cc}^D)/4$	−0.017(3)	−0.033	−0.031
N[d]	30		
σ[e]	0.002		

[a]B3LYP-D3/Def2-TZVP.

[b]MP2/aug-cc-pVTZ.

[c]Error in the unit of the last digit.

[d]Number of lines in the fit.

[e]Standard deviation of the fit.

Table 3

Planar moments of inertia of DEHA and its monosubstituted isotopologues.

	M_{aa}/uÅ^2	M_{bb}/uÅ^2	M_{cc}/uÅ^2
Parent	235.391	51.667	14.759
^{2}H	235.386	55.113	14.972
^{15}N	235.377	51.664	14.821
^{13}C$_\alpha$	236.829	52.112	14.839
^{13}C$_\beta$	241.447	51.673	14.855

Table 4

Experimental substitution coordinates (r_s) of the hydroxyl hydrogen atom of DEHA, compared to the theoretical (r_e) values.

	$|a_s|$/Å	$|b_s|$/Å	$|c_s|$/Å
r_s	i0.08(2)[a,b]	1.8555(8)	0.484(3)
	a_e/Å	b_e/Å	c_e/Å
r_e(DFT)[c]	0.000	−1.861	−0.500
r_e(MP2)[d]	0.000	−1.854	−0.497

[a]Costain's error [25] is reported in units of the last digits.

[b]This coordinate is nonzero and imaginary due to vibrational averaging.

[c]B3LYP-D3(BJ)/Def2-TZVP.

[d]MP2/aug-cc-pVTZ.

Table 5

Top panel: r_0 fitted bond distances of DEHA compared to the starting *ab initio* (MP2/aug-cc-pVTZ) r_e values. Bottom panel: shift between the r_0 and experimental rotational constants of all the involved isotopologues.

	r_0	r_e	$r_0 - r_e$
d(O-H)/Å	0.9607(33)[a]	0.9641	−0.0034
d(N-O)/Å	1.4634(3)	1.4514	0.0120
d(C-N)/Å	1.4626(3)	1.4612	0.0014
d(C-C)/Å	1.5304(5)	1.5155	0.0149
	$A_0 - A_{obs.}$ /MHz	$B_0 - B_{obs.}$ /MHz	$C_0 - C_{obs.}$ /MHz
Parent	−0.551	−0.099	−0.069
D	0.402	−0.001	−0.017
^{15}N	0.275	0.040	0.047
^{13}C$_\alpha$	−0.044	−0.104	−0.042
^{13}C$_\beta$	−0.472	0.126	0.099

[a]The error is reported in units of the last digits. Fit's root mean square on the moments of inertia is 0.010 uÅ^2.

the EFG-PAS for the 1:1 water complex of DEHA which also has a C_s-symmetry since water lies in the *bc*-plane of DEHA [7]. Actually, several isotopologues were observed, including the DEHA-H$_2^{18}$O. From the reported r_0-structure [7] the tilt angle between the I-PAS of DEHA-H$_2$O and DEHA-H$_2^{18}$O is estimated to be $\theta = 0.6°$. Using this angle as a constrain for the diagonalization of the NQC-tensors in the I-PAS of

DEHA-H$_2$O and DEHA-H$_2^{18}$O to give the same NQC-tensors in the EFG-PAS, the diagonalization angles $\theta_{DEHA-H_2O} = 25.7°$ and $\theta_{DEHA-H_2^{18}O}$

Table 6

Experimental and *ab initio* (MP2/aug-cc-pVTZ)[14]N-NQC-constants (χ) in the I-PAS and EFG-PAS, diagonalization angle (θ) and asymmetry parameter (η) of DEHA, DEDA, DEHA-H$_2$O and DEHA-H$_2^{18}$O.

	DEHA exp.	DEDA exp.	*DEHA* *MP2*	*DEDA* *MP2*	DEHA-H$_2$O exp.	DEHA-H$_2^{18}$O exp.
χ_{aa}/MHz	0.711(2)[a]	0.716(3)	0.6058	0.6058	0.664(3)	0.671(3)
χ_{bb}/MHz	5.475(3)	5.364(4)	5.3926	5.2785	−3.912(3)	−4.009(4)
χ_{cc}/MHz	−6.186(3)	−6.080(4)	−5.9984	−5.8843	3.249(2)	3.338(4)
χ_{bc}/MHz	−2.262(1)[b]	−2.524(2)[b]	−2.3445	−2.6045	4.485(3)[b]	4.409(5)[b]
θ/°	−10.6	−11.9	−11.2	−12.5	25.7[c]	25.1[c]
χ_{xx}/MHz	0.711(2)	0.716(3)	0.6058	0.6058	0.664(3)	0.671(3)
χ_{yy}/MHz	5.898(3)	5.896(4)	5.8563	5.8563	5.407(3)	5.403(5)
χ_{zz}/MHz	−6.609(3)	−6.612(4)	−6.4621	−6.4621	−6.070(3)	−6.074(5)
η	0.7849(6)	0.7834(9)	0.8125	0.8125	0.7814(8)	0.779(2)

[a]The error is reported in units of the last digits.

[b]Obtained from structural considerations (see text for details).

[c]Since DEHA-W is an oblate rotor, the diagonalization angle has been obtained as $\tan(2\theta) = 2 \cdot \chi_{bc}/(\chi_{cc} - \chi_{bb})$.

= 25.1° are obtained, respectively. The corresponding NQC-constants in the EFG-PAS are given in Table 6 with the asymmetry parameter η.

7. D-NQC constants

The experimental deuterium NQC-constants of DEDA are compared to the *ab initio* ones in Table 6. As in the case of nitrogen, since deuterium lies on the *bc*-symmetry plane, the χ_{aa} term coincides with one of the EFG-tensor components. The differences between experimental and *ab initio* values are in the order of tenths of kHz. Although these deviations are usually acceptable, because of the small values of the involved constants, the relative displacements are quite relevant (−19%, 30% and -38% for χ_{aa}, χ_{bb} and χ_{cc}, respectively). Nevertheless, we will assume that the *ab initio* diagonalization angle $\theta = 37.1°$ is correctly predicted. This hypothesis is supported by the fact that this value is very close to the angle that, according to the r_0 structure, the OD bond makes with the *c*-axis (36.0°), in agreement with an EFG directed along the bond, which is a common assumption in the case of terminal atoms (bond axis system approximation, see for instance HOD [31], CH$_3$OD [32], and CH$_3$CDO [33]). Therefore, the off-diagonal term is tentatively being estimated as:

$$\chi_{bc} = \chi_{bc}^{MP2} \cdot \frac{\chi_{bb}^{exp} - \chi_{cc}^{exp}}{\chi_{bb}^{MP2} - \chi_{cc}^{MP2}} \qquad (9)$$

The results of the subsequent diagonalization are given in the fit-1 column of Table 7 with the asymmetry parameter η. The agreement between the determined NQC-constants in the EFG-PAS and the *ab initio* ones is not satisfying, in particular, the obtained asymmetry parameter for DEDA is more than three times the *ab initio* value. For this reason, we apply a second approach, using as constrain the theoretical asymmetry parameter. The corresponding diagonalization angle is $\theta = −39.8°$ and the NQC-constants are given in the fit-2 column of Table 7. Finally, in order to fix an upper limit for the χ_{zz} value we consider the case of an EFG with perfect cylindrical symmetry for which the asymmetry parameter is exactly null. This condition corresponds to a diagonalization angle $\theta = −40.8°$ and the obtained data are given in the fit-3 column of Table 7.

8. Discussion

The plot of the *ab initio* positive and negative electrostatic potential (V) isosurfaces reported in Fig. 3, can be used as a trace to understand the EFG at the nuclei. At the orange surfaces, located along the lone pairs of the heteroatoms, the electrostatic potential is −0.5 a.u.. At the yellow surface, wrapping the whole molecule along the bonds, the electrostatic potential is +0.5 a.u.. These shapes suggest that the main EFG component at the nuclei should be roughly directed along the bonds and toward the lone pairs. Actually, considering ^{14}N in C_{3v} symmetric systems like ammonia [34], trimethylamine [35] and

Table 7

Experimental, *ab initio* (MP2/aug-cc-pVTZ) and estimated D-NQC-constants (χ) in the I-PAS and EFG-PAS, diagonalization angle (θ) and asymmetry parameter (η) of DEDA.

	exp.	*f it* − 1	*f it* − 2	*f it* − 3	*MP2*
χ_{aa}/kHz	−154(5)[a]				−183.4
χ_{bb}/kHz	43(8)				30.3
χ_{cc}/kHz	111(8)				153.1
χ_{bc}/kHz		120.2	186.3	228.5	217.1
θ/°		[−37.1][b]	−39.8	−40.8	−37.1
χ_{xx}/kHz		−48	−112.4	−154	−133.9
χ_{yy}/kHz	−154(5)				−183.4
χ_{zz}/kHz		202	266.4	308	317.3
η		0.525	[0.156]	[0]	0.156

[a]The error is reported in units of the last digits.

[b]Values in square brackets are fixed.

Table 8

Comparison of the[14]N χ_{zz} constant and asymmetry parameter of several amine compounds.

	χ_{zz}/MHz	η
NH$_3$ [34]	−4.0842(3)[a]	0
Quinuclidine [36]	−5.192(4)	0
N(CH$_3$)$_3$ [35]	−5.47(3)	0
NH$_2$OH [37]	−5.76(50)	1.0(3)
CH$_3$NHOH [38]	−6.34(30)	0.4(1)
DEHA	−6.609(3)	0.785(1)
DEHA-H$_2$O	−6.071(6)	0.781(1)

[a]The error is reported in units of the last digits.

quinuclidine [36], the *z*-axis is exactly along the lone pair direction. In the case of DEHA, the insertion of a hydroxyl group induces a rotation of the EFG-PAS towards the OH itself: looking at the *y* and *z*-axes represented in Fig. 4, we can see that their orientation is between the nitrogen lone pair and the NO bond. The same effect has been observed for hydroxylamine [37].

In Table 8 we compare the NQC-constants in the EFG-PAS, of several ammonia derivatives. As regards χ_{zz} an additive behaviour is observed. From ammonia to trimethylamine and quinuclidine the contribution of each alkyl group is $\Delta_R \simeq 0.46$ and 0.37 MHz, respectively. Overall we could attribute a shift of 0.4 MHz for every hydrogen to alkyl substitution. Comparing ammonia to hydroxylamine, the shift due to the hydroxyl is $\Delta_{OH} \simeq 1.7$ MHz. Using these data, the estimated values for the *N*-methylhydroxylamine and DEHA are −6.2 and −6.6 MHz, respectively, in good agreement with the observed ones (−6.3 and −6.6 MHz, respectively).

When water and DEHA interact to form a 1:1 molecular complex, the NQC-constant absolute values decrease, suggesting that the electric field varies less when the nitrogen lone pair is involved in a hydrogen bond. In particular, since the nitrogen lone pair roughly lies along
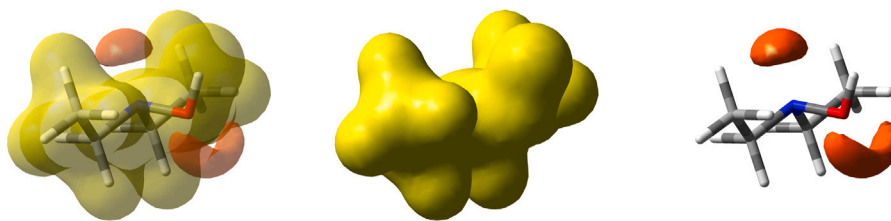
Fig. 3. Electrostatic potential isosurfaces at 0.05 a.u. (yellow) and −0.05 a.u. (orange) for DEHA (MP2/aug-cc-pVTZ).
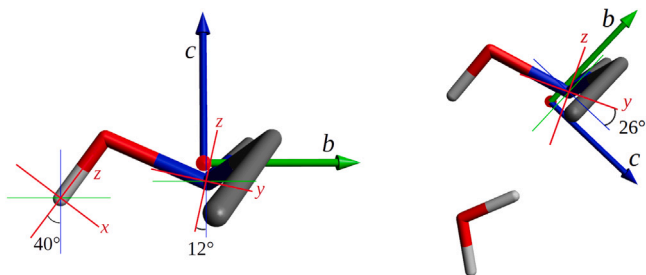

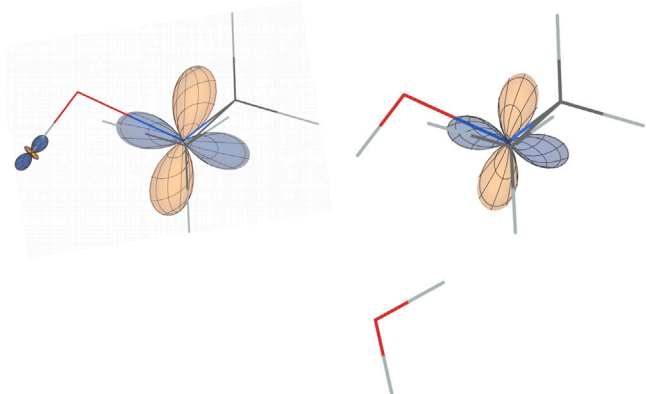**Fig. 4.** Principal inertial and electric field gradient axis systems of DEDA and DEHA-water.

Fig. 5. Polar plots of the EFG tensors of DEDA and DEHA-water at the ^{14}N and D nuclei. Blue = positive, orange = negative field gradient.

Table 9

Comparison of the D χ_{zz} constant and asymmetry parameter of several compounds.

	χ_{zz}/kHz	η
HC(O)D [41]	171(5)[a]	0.01(4)
CH$_3$C(O)D [42]	163(2)	0.04(3)
NH$_2$D [43]	282(12)	0.05(6)
HOD [31]	307.9(1)	0.135(1)
CH$_3$OD [32]	303(12)	[0][b]
HCOOD [41]	272(3)	0.08(1)
trans-i-PrOD [33]	269(4)[c]	0.10(5)
DEDA	266.4(1)	[0.156][b]

[a] The error is reported in units of the last digits.

[b] Values in square brackets are fixed.

[c] The χ_{cc} value is reported, since, fortuitously, the I-PAS and bond axis system almost coincide.

ammonia shows that the χ_{zz} of ammonia is of the same order of magnitude but it is much more symmetric. A graphical visualization of EFG tensors determined for DEHA and DEHA-W is given in Fig. 5, where the extent of the lobes is proportional to the EFG at the nuclei and the colour depends on the sign.

9. Conclusions

The rotational spectrum of DEDA has been measured and assigned for the first time. Using the determined rotational constants and literature information on other isotopolgues of DEHA, a partial r_0 structure has been determined. The high resolution of the PJ-FTMW spectrometer has allowed for resolving the hyperfine structure due to the nuclear quadrupole interaction of both ^{14}N and D and determining the corresponding diagonal NQC-constants in the I-PAS. Despite the lack of information on the off-diagonal term, based on structure variation upon isotopic substitution, the NQC-constants in the EFG-PAS could be derived for ^{14}N in DEHA and its 1:1 complex with water. It has been shown that upon hydrogen bonding χ_{zz} decreases. Comparison with other amino derivatives has evidenced that a rough additive model can be applied to estimate χ_{zz}, depending on the involved substituents. As regards the hydroxyl deuterium, an upper limit for the χ_{zz} has been determined using the bond axis approximation and a slightly smaller value has been determined constraining the asymmetry parameter to the *ab initio* value. Comparison with the little information on other available compounds shows that the EFG at the deuterium in DEDA is similar to that of other hydroxyl compounds.

CRediT authorship contribution statement

Filippo Baroncelli: Validation, Formal analysis, Investigation, Data curation, Writing – original draft, Writing – review & editing, Visualization. **Gabriele Panizzi:** Investigation, Data curation, Visualization. **Luca Evangelisti:** Validation, Formal analysis, Investigation, Resources, Data curation, Writing – review & editing, Funding acquisition. **Sonia Melandri:** Validation, Formal analysis, Investigation, Resources, Data curation, Writing – review & editing, Funding acquisition. **Assimo Maris:** Conceptualization, Validation, Formal analysis, Investigation, Resources, Data curation, Writing – original draft, Writing – review & editing, Visualization, Supervision, Funding acquisition.

the z-axis, the $|\chi_{zz}|$ decrease (0.6 MHz) is a clear diagnostic of the lone pair being sharied with the water proton. It is worth noting that the same displacement has been observed in the pyridine-ammonia complex [39] for the pyridine nitrogen atom upon formation of a hydrogen bond with one of the ammonia hydrogen atoms, whereas a smaller displacement (0.22 MHz) has been measured in the pyridine-formaldehyde complex [40] due to a $n \rightarrow \pi^*$ interaction. However, the orientation of the EFG-PAS is essentially unchanged, being the angle between the z-axis and the NO bond about 10.5° for both DEHA and DEHA-W.

Let us consider now the behaviour of the hydroxyl deuterium. Looking at the electrostatic potential surface (Fig. 3) the bond-axis system approximation seems reliable. In fit-3 we assumed a perfect cylindrical shape of the EFG, obtaining χ_{zz} = 308 kHz. This value is very close to that determined for methanol-OD [32] using the same approximation: χ_{zz} = 303 kHz. However, fixing the asymmetry parameter to the *ab initio* value (fit-2), χ_{zz} results to be similar to those of *trans-iso*-propanol-OD [33] and formic acid-OD [41], as it can be seen in Table 9. For this series of compounds, χ_{zz} is slightly smaller than that of monodeuterated water but almost double those of formaldehyde-d_1 [41] and acetaldehyde-d_1 [42] where deuterium is bound to a sp^2 carbon atom instead of to an oxygen atom. Comparison with monodeuterated

Declaration of competing interest

The authors declare that they have no known competing financial interests or personal relationships that could have appeared to influence the work reported in this paper.

Data availability

The used data are given in the manuscript.

Acknowledgements

References

[1] J. Nicolas, Y. Guillaneuf, C. Lefay, D. Bertin, D. Gigmes, B. Charleux, Nitroxide-mediated polymerization, Prog. Polym. Sci. 38 (1) (2013) 63–235, http://dx.doi.org/10.1016/j.progpolymsci.2012.06.002.

[2] J.L. Hodgson, M.L. Coote, Clarifying the mechanism of the Denisov cycle: How do hindered amine light stabilizers protect polymer coatings from photo-oxidative degradation? Macromolecules 43 (10) (2010) 4573–4583, http://dx.doi.org/10.1021/ma100453d.

[3] G. Audran, P. Brémond, S.R.A. Marque, Labile alkoxyamines: past, present, and future, Chem. Commun. 50 (2014) 7921–7928, http://dx.doi.org/10.1039/C4CC01364F.

[4] R.G. Hicks, What's new in stable radical chemistry? Org. Biomol. Chem. 5 (2007) 1321–1338, http://dx.doi.org/10.1039/B617142G.

[5] G. Audran, P. Brémond, J.-M. Franconi, S.R. Marque, P. Massot, P. Mellet, E. Parzy, E. Thiaudière, Alkoxyamines: a new family of pro-drugs against cancer. Concept for theranostics, Org. Biomol. Chem. 12 (5) (2014) 719–723, http://dx.doi.org/10.1039/c3ob42076k.

[6] G. Salvitti, E. Pizzano, F. Baroncelli, S. Melandri, L. Evangelisti, F. Negri, M. Coreno, K.C. Prince, A. Ciavardini, H. Sa'adeh, M. Pori, M. Mazzacurati, A. Maris, Spectroscopic and quantum mechanical study of a scavenger molecule: N,N-diethylhydroxylamine, Spectrochim. Acta A 281 (2022) 121555, http://dx.doi.org/10.1016/j.saa.2022.121555.

[7] G. Salvitti, F. Baroncelli, C. Nicotri, L. Evangelisti, S. Melandri, A. Maris, How water interacts with the NOH group: The rotational spectrum of the 1:1 N,N-diethylhydroxylamine.water complex, Molecules 27 (2022) 8190, http://dx.doi.org/10.3390/molecules27238190.

[8] D. Lv, A. Maris, L. Evangelisti, A. Maggio, W. Song, A.A. Elliott, S.A. Peebles, J.L. Neill, M.T. Muckle, B.H. Pate, R.A. Peebles, S. Melandri, σ–Hole activation and structural changes upon perfluorination of aryl halides: direct evidence from gas phase rotational spectroscopy, Phys. Chem. Chem. Phys. 23 (2021) 18093–18101, http://dx.doi.org/10.1039/D1CP03023J.

[9] J.-U. Grabow, W. Stahl, H. Dreizler, A multioctave coaxially oriented beam-resonator arrangement Fourier-transform microwave spectrometer, Rev. Sci. Instrum. 67 (12) (1996) 4072–4084, http://dx.doi.org/10.1063/1.1147553.

[10] T. Balle, W. Flygare, Fabry-Perot cavity pulsed Fourier transform microwave spectrometer with a pulsed nozzle particle source, Rev. Sci. Instrum. 52 (1) (1981) 33–45, http://dx.doi.org/10.1063/1.1136443.

[11] W. Caminati, L. Evangelisti, G. Feng, B.M. Giuliano, Q. Gou, S. Melandri, J.-U. Grabow, On the Cl...C halogen bond: a rotational study of CF_3Cl–CO, Phys. Chem. Chem. Phys. 18 (2016) 17851–17855, http://dx.doi.org/10.1039/C6CP01059H.

[12] F. Weigend, R. Ahlrichs, Balanced basis sets of split valence, triple zeta valence and quadruple zeta valence quality for H to Rn: Design and assessment of accuracy, Phys. Chem. Chem. Phys. 7 (2005) 3297–3305, http://dx.doi.org/10.1039/B508541A.

[13] A.D. Becke, Density-functional thermochemistry. III. The role of exact exchange, J. Chem. Phys. 98 (1993) 5648–5652, http://dx.doi.org/10.1063/1.464913.

[14] C. Lee, W. Yang, R.G. Parr, Development of the Colle-Salvetti correlation-energy formula into a functional of the electron density, Phys. Rev. B 37 (1988) 785–789, http://dx.doi.org/10.1103/PhysRevB.37.785.

[15] S. Grimme, J. Antony, S. Ehrlich, H. Krieg, A consistent and accurate ab initio parametrization of density functional dispersion correction (DFT-D) for the 94 elements H-Pu, J. Chem. Phys. 132 (2010) 154104, http://dx.doi.org/10.1063/1.3382344.

[16] S. Grimme, S. Ehrlich, L. Goerigk, Effect of the damping function in dispersion corrected density functional theory, J. Comput. Chem. 32 (7) (2011) 1456–1465, http://dx.doi.org/10.1002/jcc.21759.

[17] T.H. Dunning Jr., Gaussian basis sets for use in correlated molecular calculations. I. the atoms boron through neon and hydrogen, J. Chem. Phys. 90 (2) (1989) 1007–1023, http://dx.doi.org/10.1063/1.456153.

[18] C. Møller, M.S. Plesset, Note on an approximation treatment for many-electron systems, Phys. Rev. 46 (7) (1934) 618, http://dx.doi.org/10.1103/PhysRev.46.618.

[19] J. Autschbach, S. Zheng, R.W. Schurko, Analysis of electric field gradient tensors at quadrupolar nuclei in common structural motifs, Concepts Magn. Reson. A 36A (2) (2010) 84–126, http://dx.doi.org/10.1002/cmr.a.20155.

[20] I. Wolfram Research, Mathematica, Version 13.1, Champaign, IL, 2022, URL https://www.wolfram.com/mathematica.

[21] H.M. Pickett, The fitting and prediction of vibration-rotation spectra with spin interactions, J. Mol. Spectrosc. 148 (2) (1991) 371–377, http://dx.doi.org/10.1016/0022-2852(91)90393-O.

[22] J. Watson, Vibrational Spectra and Structure, Elsevier, New York/Amsterdam, 1977.

[23] P. Pyykkö, Year-2017 nuclear quadrupole moments, Mol. Phys. 116 (10) (2018) 1328–1338, http://dx.doi.org/10.1080/00268976.2018.1426131.

[24] P. Pyykkö, Spectroscopic nuclear quadrupole moments, Mol. Phys. 99 (19) (2001) 1617–1629, http://dx.doi.org/10.1080/00268970110069010.

[25] C.C. Costain, Determination of molecular structures from ground state rotational constants, J. Chem. Phys. 29 (1958) 864–874, http://dx.doi.org/10.1063/1.1744602.

[26] J. Kraitchman, Determination of molecular structure from microwave spectroscopic data, Amer. J. Phys. 21 (1953) 17–25, http://dx.doi.org/10.1119/1.1933338.

[27] O. Takeshi, On negative inertial defect, J. Mol. Struct. 352–353 (1995) 225–233, http://dx.doi.org/10.1016/0022-2860(95)08844-L.

[28] V.W. Laurie, Note on the determination of molecular structure from spectroscopic data, J. Chem. Phys. 28 (4) (1958) 704–706, http://dx.doi.org/10.1063/1.1744218, URL http://dx.doi.org/10.1744218.

[29] Z. Kisiel, Least-squares mass-dependence molecular structures for selected weakly bound intermolecular clusters, J. Mol. Spectrosc. 218 (2003) 58–67, http://dx.doi.org/10.1016/S0022-2852(02)00036-X.

[30] Z. Kisiel, PROSPE-Programs for ROtational SPEctroscopy URL https://www.ifpan.edu.pl/~kisiel/prospe.htm.

[31] H. Bluyssen, J. Verhoeven, A. Dymanus, Hyperfine structure of HDO and D_2O by beam maser spectroscopy, Phys. Lett. 25 (3) (1967-8) http://dx.doi.org/10.1016/0375-9601(67)90864-X.

[32] K. Casleton, S. Kukolich, Measurement of deuterium quadrupole coupling in CH_3OD, Chem. Phys. Lett. 22 (2) (1973) 331–334, http://dx.doi.org/10.1016/0009-2614(73)80105-8.

[33] E. Hirota, Y. Kawashima, Internal rotation of the hydroxyl group in isopropanol and the chirality of the gauche form: Fourier transform microwave spectroscopy of $(CH_3)_2CHOD$, J. Mol. Spectrosc. 207 (2) (2001) 243–253, http://dx.doi.org/10.1006/jmsp.2001.8352.

[34] G.R. Gunther-Mohr, R.L. White, A.L. Schawlow, W.E. Good, D.K. Coles, Hyperfine structure in the spectrum of $N^{14}H_3$. I. experimental results, Phys. Rev. 94 (1954) 1184–1191, http://dx.doi.org/10.1103/PhysRev.94.1184.

[35] D.R. Lide, D.E. Mann, Microwave spectra of molecules exhibiting internal rotation. III. trimethylamine, J. Chem. Phys. 28 (4) (1958) 572–576, http://dx.doi.org/10.1063/1.1744194.

[36] D. Consalvo, W. Stahl, Rotational spectrum and structure of the quinuclidine–water complex, J. Mol. Spectrosc. 174 (2) (1995) 520–535, http://dx.doi.org/10.1006/jmsp.1995.0020.

[37] S. Tsunekawa, Microwave spectrum of hydroxylamine, J. Phys. Soc. Japan 33 (1) (1972) 167–174, http://dx.doi.org/10.1143/JPSJ.33.167.

[38] E.-M. Sung, M.D. Harmony, Microwave spectrum, structure, quadrupole coupling constants, dipole moment, and barrier to internal rotation of N-methylhydroxylamine, J. Mol. Spectrosc. 74 (2) (1979) 228–241, http://dx.doi.org/10.1016/0022-2852(79)90054-7.

[39] L. Spada, N. Tasinato, F. Vazart, V. Barone, W. Caminati, C. Puzzarini, Non-covalent interactions and internal dynamics in pyridine–ammonia: A combined quantum-chemical and microwave spectroscopy study, Eur. J. Chem. 23 (20) (2017) 4876–4883, http://dx.doi.org/10.1002/chem.201606014.

[40] S. Blanco, J.C. López, Rotational characterization of an $n \to \pi^*$ interaction in a pyridine–formaldehyde adduct, J. Phys. Chem. Lett. 9 (16) (2018) 4632–4637, http://dx.doi.org/10.1021/acs.jpclett.8b01719.

[41] D.J. Ruben, S.G. Kukolich, Deuterium quadrupole coupling in formic acid, J. Chem. Phys. 60 (1) (1974) 100–102, http://dx.doi.org/10.1063/1.1680754.

[42] L. Martinache, A. Bauder, Microwave spectrum of acetaldehyde-1-d1: Deuterium quadrupole splittings and internal rotation analysis, Chem. Phys. Lett. 164 (6) (1989) 657–663, http://dx.doi.org/10.1016/0009-2614(89)85277-7.

[43] P. Thaddeus, L.C. Krisher, P. Cahill, Hyperfine structure in the microwave spectrum of NH_2D, J. Chem. Phys. 41 (6) (1964) 1542–1547, http://dx.doi.org/10.1063/1.1726119.